Received: 25 May 2021 | Revised: 7 October 2021 | Accepted: 22 November 2021

DOI: 10.1002/eqe.3589

RESEARCH ARTICLE

WILEY

Non-linear dynamic analysis of buildings founded on piles: Simplified modelling strategies for soil-foundation-structure interaction

Fabrizio Noto[1] | **Maria Iovino**[2] | **Raffaele Di Laora**[3] | **Luca de Sanctis**[2] | **Paolo Franchin**[4]

[1] METIS s.r.l., Roma, Italy

[2] Università di Napoli Parthenope, Napoli, Italy

[3] Università della Campania Luigi Vanvitelli, Aversa (CE), Italy

[4] Sapienza Università di Roma, Roma, Italy

Correspondence
Raffaele Di Laora, Università della Campania Luigi Vanvitelli, Aversa (CE), Italy.
Email: raffaele.dilaora@unicampania.it

Funding information
Dipartimento della Protezione Civile; Italian civil protection

Abstract

The paper investigates the problem of Soil-Foundation-Structure Interaction (SFSI) for buildings supported on piles through the comparative analysis between the fixed base and the compliant base assumptions. The structure, a nine-storey residential building (with or without infills), is modelled in non-linear regime while the piled foundation is idealized by means of independent lumped parameters models, either linear or non-linear. In this last case, the soil-foundation system is replaced by an assembly of viscous-dampers, fictitious masses and non-linear springs modelled according to the classical Bouc-Wen formulation, so as to account for the hysteretic behaviour of the foundation. A detailed calibration procedure for both linear and non-linear foundation models is also presented and discussed. Two different natural soil deposits are considered, a pyroclastic deposit and a deep layer of lacustrine clay. The results undertaken in the context of a probabilistic analysis show that SFSI may lead to a significant reduction of the seismic demand in infilled buildings at low and intermediate earthquake intensity levels. Conversely, at higher intensity earthquakes the seismic demand is not affected by the non-linear springs. It is shown that a proper modelling of radiation mechanism at foundation level is crucial for a reliable and sustainable prediction of SFSI effects.

KEYWORDS

foundation impedance, inertial interaction, pile groups, replacement oscillator

1 | INTRODUCTION

The seismic demand in buildings founded on piles is usually evaluated by neglecting the effects owing to the foundation compliance, that is, the elongation of the structural period and the energy dissipation associated to the oscillation motion of the foundation. Such an assumption is due to the widespread belief that the fixed base assumption is reasonable, considering that piled foundations are much less compliant than shallow foundations with comparable plan dimensions.

However, this argument neglects that the radiation mechanism is completely different for piles, which usually provide higher dissipation. Also, plastic deformations concentrating in the soil within the piles are an important source of dissipation, especially in case of high intensity earthquakes.

Foundation compliance is both frequency and intensity dependent. The simplest way to idealize the behaviour of the complete soil-foundation-structure system is that represented by the equivalent oscillator as originally introduced by Veletsos and Meek[1] and Veletsos and Nair,[2] which consider the soil-foundation properties at the resonance frequency of the whole system. Based on this linear-elastic model, Bilotta et al.[3] have investigated the dynamic behaviour of a tall building supported by unevenly distributed large diameter piles, concluding that the compliance of the piled foundation may reduce the spectral acceleration by 15%. A more refined approach, yet computationally more expensive, is that of replacing the soil-foundation system with frequency-dependent springs and dashpots.[4] This model has been applied by Makris et al.[5] to the case history of Painter Street Bridge, a continuous two-span cast-in-place pre-stressed bridge in northern California, shaken in 1992 by the 7.1 M_w Petrolia earthquake. The same methodology has been recently employed by de Sanctis et al.[6] to quantify the relevance of the SFSI for the dynamic response of piles-supported buildings. The authors found a remarkable reduction of the structural displacement compared to that of the fixed base model especially in soft soils, where the addition of piles is the most common design option to improve the serviceability performance of shallow foundations.[7] Note that, while the replacement oscillator by Veletsos and Meek[1] can be solved in the time domain, the Parmelee[4] model requires the solution of the equations of motion in the frequency domain.

An alternative approach for time domain analyses is that of replacing the soil-foundation system with suitable Lumped Parameter Models (LPMs),[8] thus reproducing the frequency-dependent behaviour of the foundation impedances through an assembly of viscous dampers, elastic springs and fictitious masses. This class of models has, since then, considerably evolved and has been generalized to accurately reproduce even complex frequency-dependent impedances.[9]

The main advantage of performing inertial interaction analysis in the time-domain is the possibility to account for the non-linearity of the structural members. This analysis technique has been applied by Pinto and Franchin[10] who employed the coupled translational-rotational LPM by Taherzadeh et al.[11] to examine the response of a 450 m long multispan bridge supported by reinforced concrete piers enhanced by groups of six (or eight) large diameter piles and subjected to either synchronous or asynchronous input motions. They found a small decrease of the structural response in comparison to that determined through the fixed base assumption. The same technique has been applied to examine the seismic performance of a plane, six storey-four bay, reinforced concrete wall frame dual system by Carbonari et al.[12] and a plane, six storey-three bay, reinforced concrete frame by Carbonari et al.[13] In both cases, SFSI led to a worse behaviour in terms of lateral displacement. While the maximum difference between the lateral displacements in compliant and fixed base models was 23% for the wall-frame dual system, the detrimental effect of SFSI for the three bay structure was of minor concern. This outcome, however, is not in line with the statistical trend of beneficial SFSI effects for pile-supported structures. As explained by authors, the detrimental effect of SFSI is due to the rocking component of the foundation input motion induced by pile-soil kinematic interaction. As a matter of fact, both the structures were founded on mono-piles, with the exception of the wall belonging to the dual system, whose foundation was a 3×1 group of piles. For this particular piles' layout (mono-piles and/or very small pile groups) the rocking motion induced by kinematic interaction may be important, as outlined also by Sextos et al.[14] For common piles' layouts the effect of the rocking component of the foundation motion is instead negligible[15] and SFSI usually leads to a reduction of the seismic demand. This is also consistent with common expectations encoded in design documents such as Eurocode EN-1998-5,[16] claiming that *'for the majority of common building structures, the effects of soil-structure-interaction tend to be beneficial, since they reduce the bending moment and shear forces in the various member of the superstructure'*.

The foregoing studies have focused primarily on the case of linear visco-elastic behaviour of the piled foundation. Yet impedance functions can be adopted to simulate approximately non-linear effects. Goit et al.[17] have distinguished between 'global' and 'local' non linearity, with the former being the soil non linearity induced by upward propagating waves and the latter owing to the concentration of plastic strains around the pile. While the global source can be managed through the 'equivalent linear' analysis, the treatment of local non linearity is far more complicated and requires adjusted dynamic pile-to-pile interaction factors when using superposition. Based on experimentally measured horizontal interaction factors, Goit et al. have proven that the superposition approach, in which the interplay between any pair of piles is evaluated without considering the neighbouring piles, is applicable at low and intermediate earthquake intensities. Conversely, at high intensity levels plastic strains concentrate in a wider area and this causes in turn a leftward shift of the resonance frequency of the foundation. Such an effect, referred to as 'group' non linearity can be hardly modelled by the superposition approach. After all, one would expect that, to an extent that depends on the conservatism of the foundation design, for high intensity earthquakes the soil-foundation system would experience a non-linear response. Accordingly, the soil-foundation system should also be non-linear so as to be consistent with the complexity of the constitutive assumption

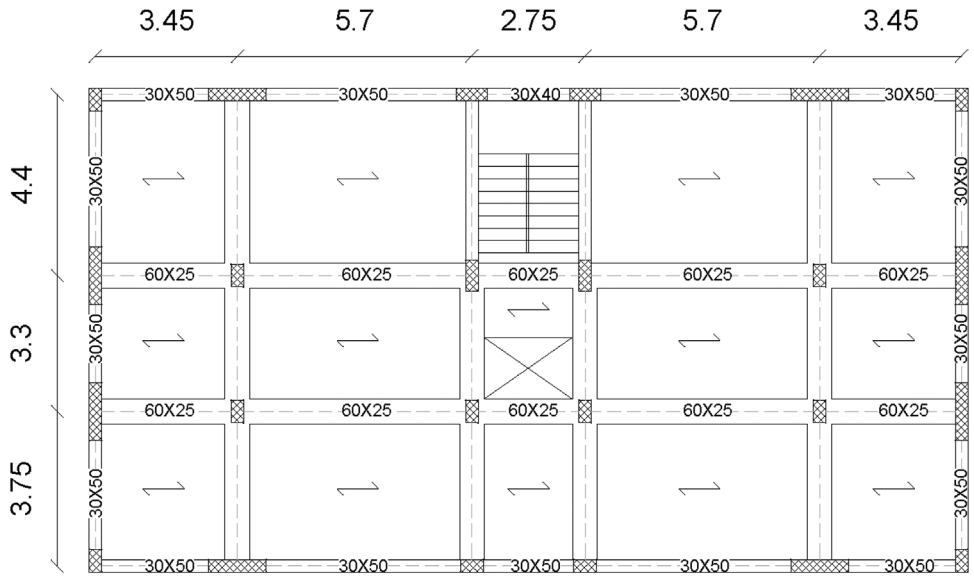

FIGURE 1 Plan view of the reference building

made to idealize the structure. This paper is thus primarily aimed at investigating the mechanism of dynamic SFSI for pile supported buildings in which the non-linear behaviour of the foundation is explicitly modelled. In this respect, it builds up appropriately on previous literature works on this subject. Obviously, a possible option would be the direct approach,[18–21] that is, to create a Finite Element (FE) model of the structure, the foundation and the geological media, extending to an appropriate horizontal distance and depth from the foundation and equipped with transmitting boundaries, so as to absorb outgoing waves emitted by the foundation. This approach, however, is computationally expensive and thereby not suitable to carry out several hundreds of inelastic response-history analyses, such as those performed in this study in the context of the Multiple Stripe Analysis strategy. Therefore, the SFSI problem is here addressed by replacing the soil-foundation system with a simplified non-linear inertial macro-element (N-LIME) consisting of a lumped plasticity model at the superstructure-foundation interface modelling the inelastic response in the pile-soil system, plus a mass to reproduce frequency-dependence and a viscous damper to model the energy dissipated through radiation. More specifically, for the non-linear spring portion of this model, reference is made to the Bouc-Wen (BW)[22,23] hysteretic model in any oscillation mode of the foundation. The coupling between rotational and translational vibrations is disregarded, as its consideration is felt to be of little importance. The N-LIME can be viewed as the non-linear extension of a LPM, with the advantage of eliminating the need to calibrate a different LPM for each intensity level of earthquake.

The results of the analyses carried out with the proposed model are compared with those obtained using: (a) the fixed base assumption; (b) visco-elastic LPMs, in which non-linearity in the pile-soil system is not accounted for, but translation-rotation coupling is; (c) the N-LIME model; (d) the N-LIME without fictitious mass, to shed light on the importance of the frequency dependence of the foundation stiffness; (e) the BW model (i.e., the N-LIME with neither fictitious mass nor damper), to account only for the non-linear behaviour of the foundation. The discussion is developed based on the results obtained at three different intensity levels of earthquakes selected from a complete seismic risk analysis carried out according to the MSA approach, with reference to a nine-storey residential building founded on two subsoils, a pyroclastic deposit from the eastern area of Napoli, and a soft clay profile from Piana del Fucino (L'Aquila).

2 | CASE STUDIES

2.1 | Reference building models and soil properties

The reference building examined in this work is a nine-storey residential apartment building with a wall earthquake-resistant system (walls carry out more than 65% of the total base shear). Shear walls are concentrated along the periphery of the floor area in a double symmetrical arrangement, as depicted in Figure 1. The building was designed according to Italian Building Code NTC 2008[24] with reference to the sites of Napoli and L'Aquila (Italy). Three configurations of masonry infills were considered (Figure 2): (a) Bare Frame (BF); (b) Infilled Frame (IF); (c) Pilotis Frame (PF). For (a),

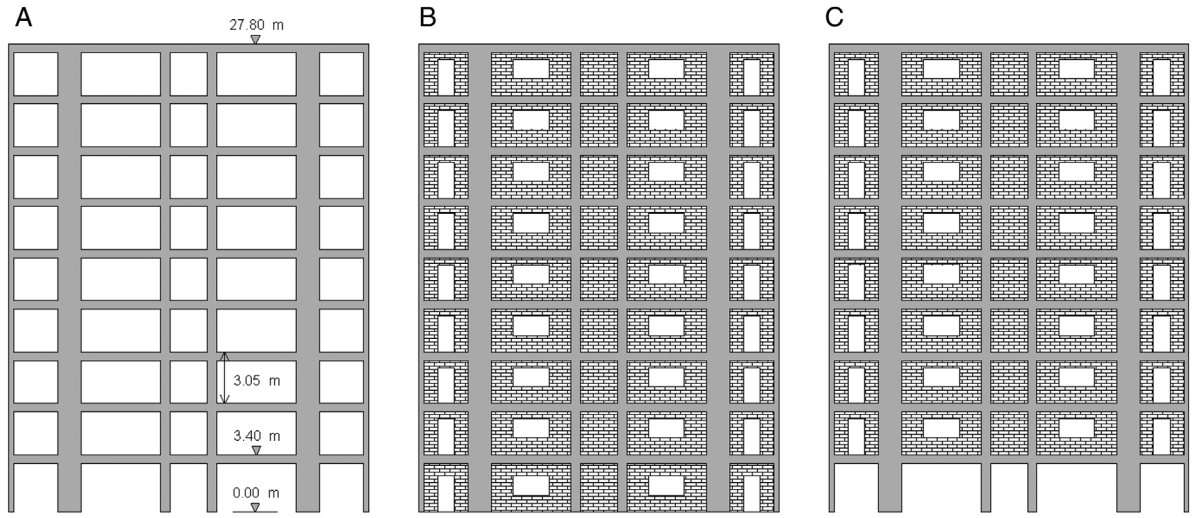

FIGURE 2 Building models considered in the analyses: (A) Bare Frame (BF), (B) infilled frame (IF), (C) Pilotis Frame (PF)

TABLE 1 Oscillation periods and participating masses for building models bare frame (BF), infilled frame (IF) e, pilotis frame (PF)

#	#	Naples			L'Aquila		
Building	Transl. vibration modes	T [s]	m_x [%]	m_y [%]	T [s]	m_x [%]	m_y [%]
BF	1	1.665	77	0	1.538	76	0
	2	1.433	0	78	1.278	0	77
	3	0.519	11	0	0.464	12	0
	4	0.45	0	11	0.395	0	12
	5	0.274	4	0	0.236	5	0
	6	0.242	0	4	0.207	0	4
IF	1	0.847	56	22	0.863	75	1
	2	0.834	22	55	0.822	1	75
	3	0.281	0	13	0.276	12	0
	4	0.274	13	0	0.271	0	13
	5	0.159	0	4	0.152	1	3
	6	0.154	4	0	0.151	4	1
PF	1	0.907	74	9	0.902	79	1
	2	0.888	9	73	0.855	1	78
	3	0.304	0	12	0.292	12	0
	4	0.299	12	0	0.285	0	13
	5	0.168	0	3	0.159	3	0
	6	0.165	3	0	0.157	0	3

infills are modelled as masses, while for (b) and (c) they are modelled also with their stiffness and strength, duly accounting for strength and stiffness reduction due to the openings. A complete description of the fixed base 3D inelastic models set up in OpenSEES[25] can be found in Ricci et al.[26] Table 1 summarizes the fundamental periods and the participating masses of the fixed base models for the selected sites. Note that the periods differ because different members' dimensions and reinforcement resulted from the same architectural layout, due to the different seismicity of the two sites (the building in L'Aquila being stronger and thus stiffer).

Figure 3 shows the subsoil layering reconstructed in the eastern area of Napoli and the shear wave velocity, V_s, profile determined from cross-hole and down-hole tests, carried out down to 60 m (Vinale 1998). Below such depth, no direct measurements were available and the V_s profile was extrapolated to about 100 m on the basis of a deep cone penetration test using a regional correlation.[27] The variation of normalized shear modulus, G/G_0, and damping ratio, D, with the

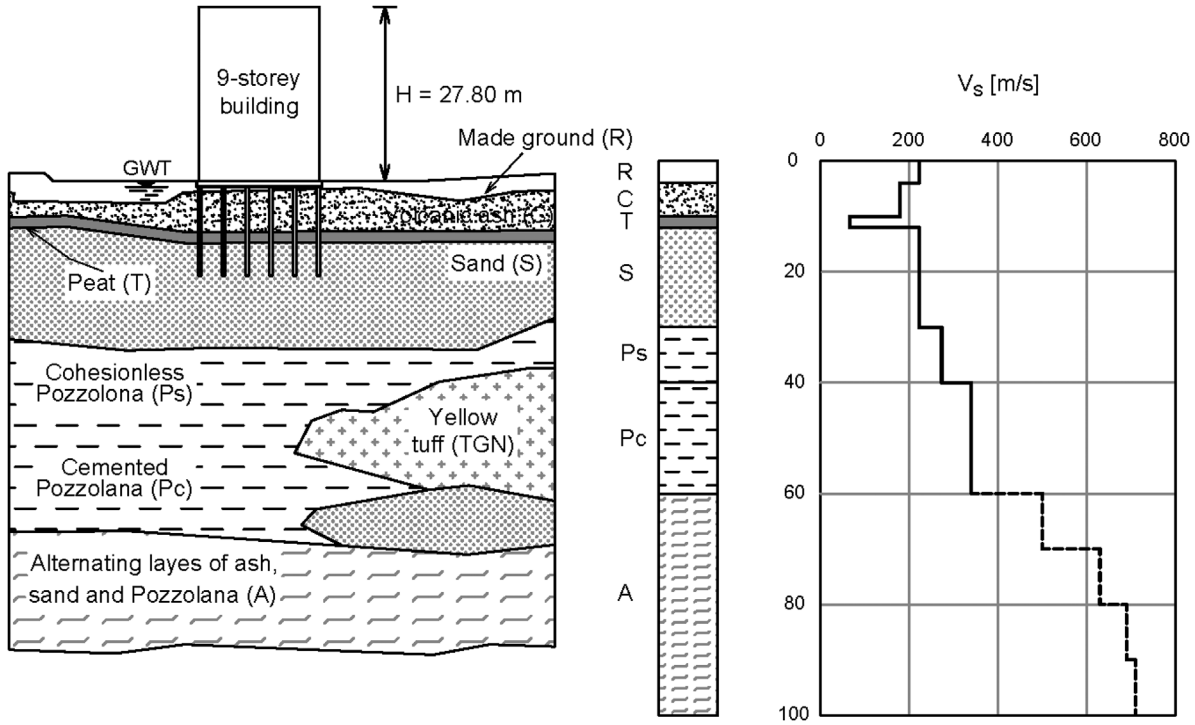

FIGURE 3 Subsoil conditions and shear wave velocity profile

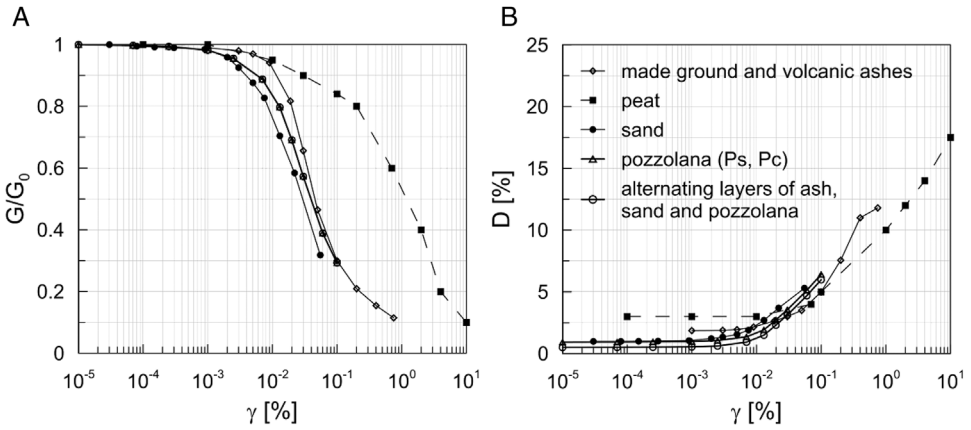

FIGURE 4 Variation of normalized shear modulus (A) and damping ratio (B) with shear strain

shear strain, γ, were defined by resonant column tests carried out on undisturbed samples of Pozzolana[28] or based on data from literature (Figure 4). Peat behaviour was characterized by using experimental data published by Wehling et al.[29] A viscoelastic bedrock was assumed at 60 m depth, with shear wave velocity V_{sb} = 800 m/s and damping ratio D = 0.5%.[3] A piled foundation consisting of 6 × 4 continuous flight auger piles 14 m long and 0.6 m in diameter uniformly spread underneath the raft was designed to meet the settlement criteria. Further details on the foundation design can be found in de Sanctis et al.[6]

The second site is Piana del Fucino (close to L'Aquila, Italy), a deep layer of very soft lacustrine clay. Site conditions were investigated by Burghignoli et al.[30] Figure 5 shows the V_s profile obtained from cross-hole, down-hole and piezocone tests, and the profile of undrained shear strength coming from cone penetration , vane and lab tests. Below 40 m no direct measurements were available and the V_s profile was extrapolated based on the correlation with the cone penetration test of Mayne and Rix,[31] assuming a linear variation of tip resistance, q_c, with depth. The variation of G/G_0, with γ was evaluated from resonant column and torsional shear tests (Figure 6). All the experimental data can be described with a very good accuracy by the relationship of Konder and Zelansko.[32] Since data on the variation of D with γ are not available, reference

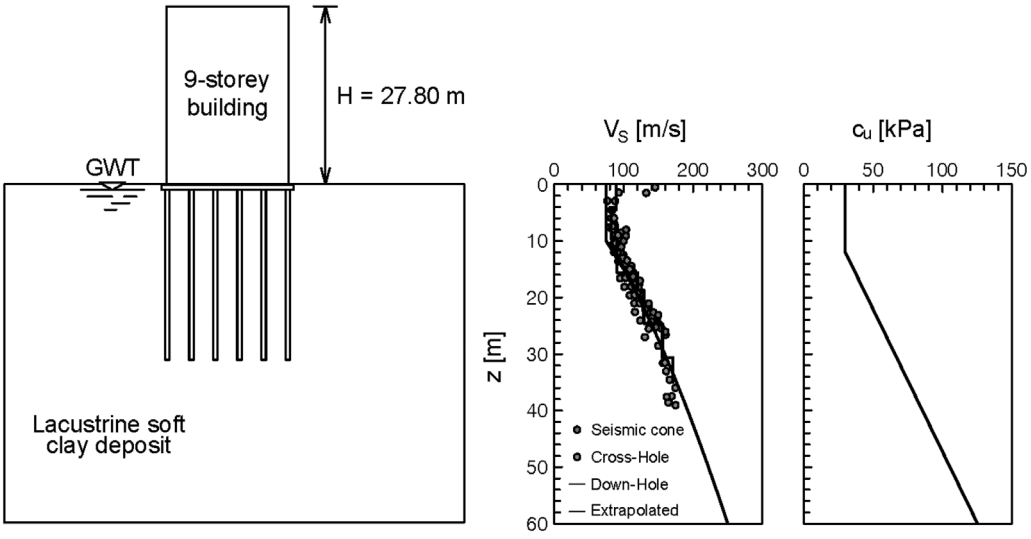

FIGURE 5 Subsoil conditions and shear wave velocity profile

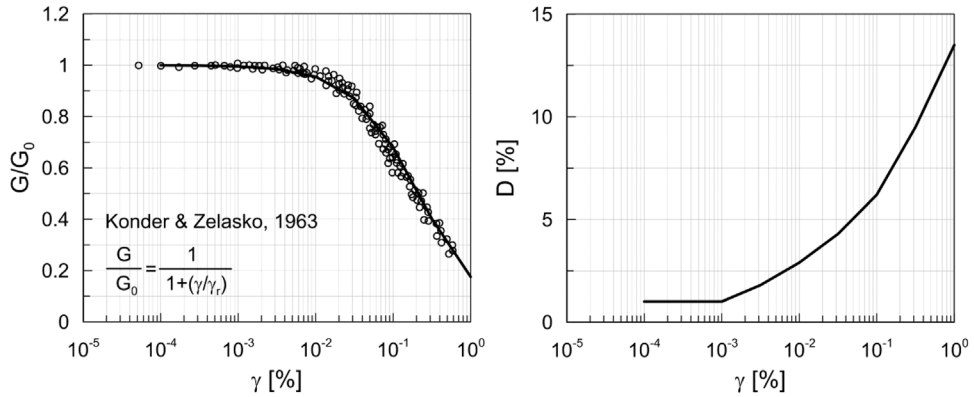

FIGURE 6 Variation of normalized shear modulus and damping ratio with shear strain

is made to the literature curve by Vucetic and Dobry[33] corresponding to the plasticity index of the clay deposit ($PI \sim 50\%$). In this case, to satisfy both settlement and capacity criteria, a layout of 6×4 continuous flight auger piles 30 m long and 0.8 m in diameter uniformly spread underneath the raft was adopted.

2.2 | Selected input signals and foundation input motion

Input signals were selected from ITACA 3.1[34] and NGA West 2[35] databases in the framework of the MSA by grouping them into Intensity Measure Levels (IMLs) ordered according to the return period, T_r, of the earthquake action. For each level, the corresponding 'stripe' of seismic demand in the building (e.g., the maximum lateral displacement or the inter-storey drift) provides support for the probabilistic characterization of the demand conditional on intensity. An application of this analysis technique to the BF model on fixed base is represented in Figure 7 for both sites of Napoli and L'Aquila, with reference to the roof displacement ratio. Note that the structure has smaller drifts in the Y direction due to the presence of the staircase and the stiffer infills with no windows on the short side. The algorithm adopted to select the signals is the Conditional Spectrum method[36] in which motions are selected so as to match the joint probability distribution of response spectral ordinates conditional to $S_a(T_1)$, T_1 being the fundamental oscillation period of the building, at each return period considered in the Multiple Stripe Analysis (Figure 8). The total amount of motions selected for the risk analysis is equal to 20 (bi-component) motions for each of the 10 intensity levels considered (Table 2), corresponding to a total of 400 records. Further details can be found in Iervolino et al.[37]

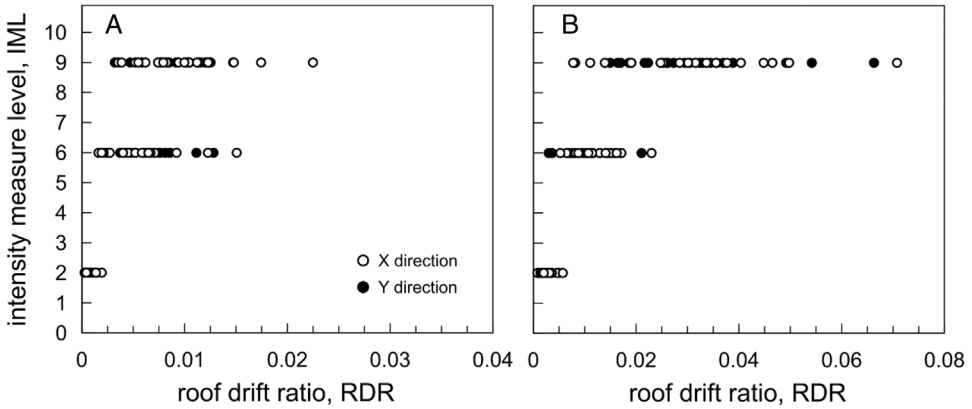

FIGURE 7 Results of the MSA for building type bare frame (BF) on fixed base and the two sites of (A) Napoli and (B) L'Aquila

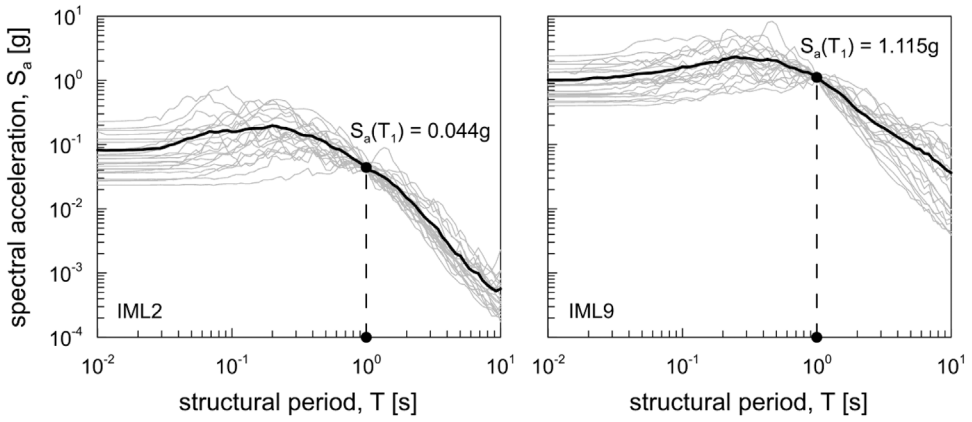

FIGURE 8 Conditional spectrum criterion

TABLE 2 Intensity measure levels (IMLs) and associated return periods

IML	Return period
	[years]
1	10
2	50
3	100
4	250
5	500
6	1000
7	2500
8	5000
9	10000
10	100000

The foundation input motion was evaluated by means of one dimensional seismic site response analysis carried out by code Strata,[38] employing the equivalent-linear approach. Ground motions recorded on outcropping rock were first deconvolved until the bedrock depth and then propagated upward through the reference subsoil model until the depth of the foundation cap, that is equivalent to impose the incoming wave in the rock medium at the base of the soil model. As outlined in de Sanctis et al.,[6] the change of seismic motion induced by pile-soil kinematic interaction was of little importance and, therefore, not considered in this study.

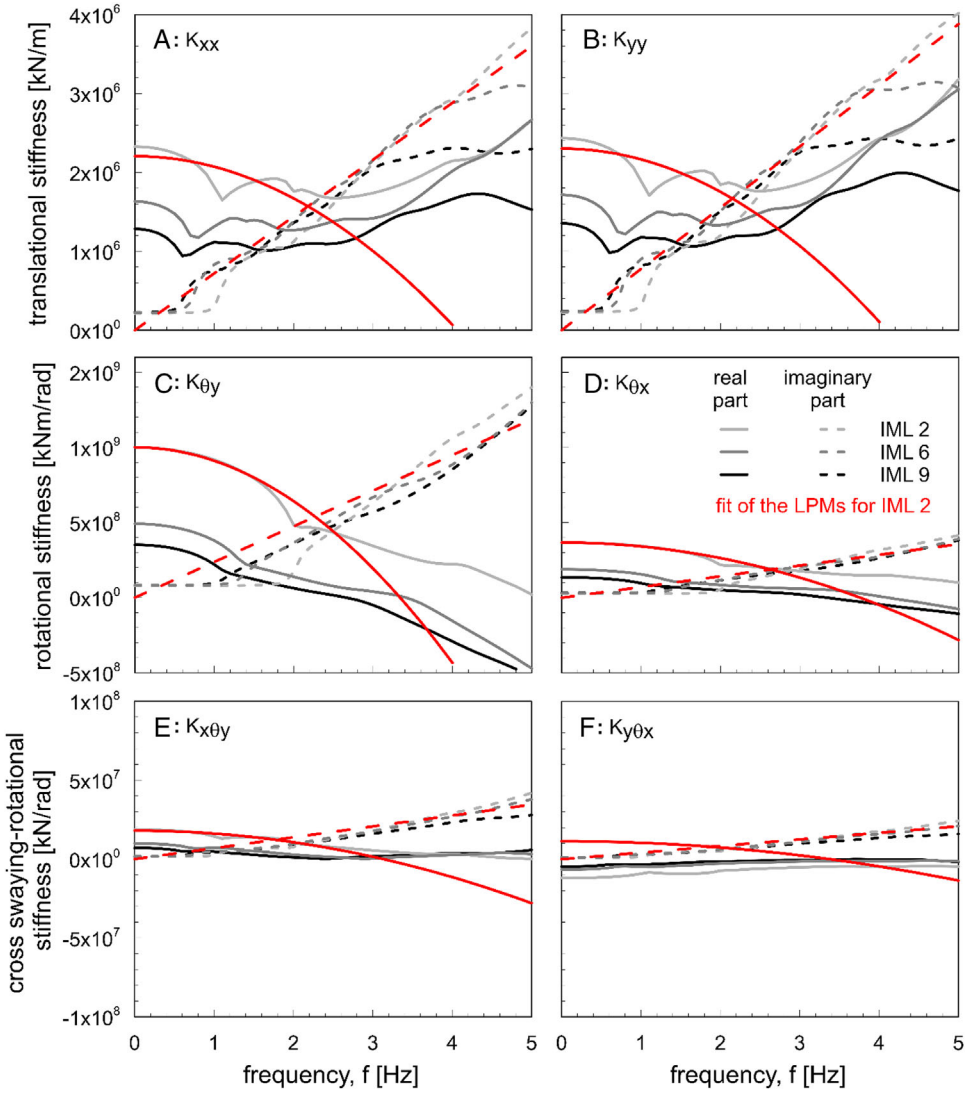

FIGURE 9 Impedance functions of the pile group for intensity measure levels (IMLs) 2, 6, and 9

3 | CALIBRATION OF SFSI MODELS

3.1 | Visco-elastic Lumped Parameter Model

The code Dynapile 3.0[39] based on the consistent boundary matrix method[40] is adopted to compute foundation impedances. Group effects are modelled by means of superposition and frequency dependent pile-to-pile interaction factors. The piles' connecting cap is supposed to be rigid and clear from the soil. Kausel et al.[41] have shown that most of non-linearity occurs as a result of the earthquake motion and not as a result of soil-structure interaction. Thus, the soil properties consistent with the mobilized free-field strain levels may be also used without further modification to account for the additional soil motion imposed by the oscillation of the structure. Based on the above, a set of impedance functions was evaluated for each IML adopting as starting point the average shear stiffness and damping ratio profiles mobilized by the passage of seismic waves. Only 'global' non linearity as defined by Goit et al.[17] was hence accounted for. Notably, piles spacing ratio (s/d) is 4.7-5.3 for layout of Piana del Fucino and even larger for the piled foundation of Naples, so as 'local' nonlinear effects are expected to not affect pile-to-pile interplay. Figure 9 shows the real and imaginary parts of the translational, rotational and cross swaying-rotational impedance functions of the pile group for IMLs 2, 6 and 9 and the site of Naples. The same plots pertaining to the site of Piana del Fucino are shown in Figure 10. Noticeably, the interval where the imaginary part of any function remains constant is associated to soil hysteretic damping; beyond a cut-off frequency (natural frequency

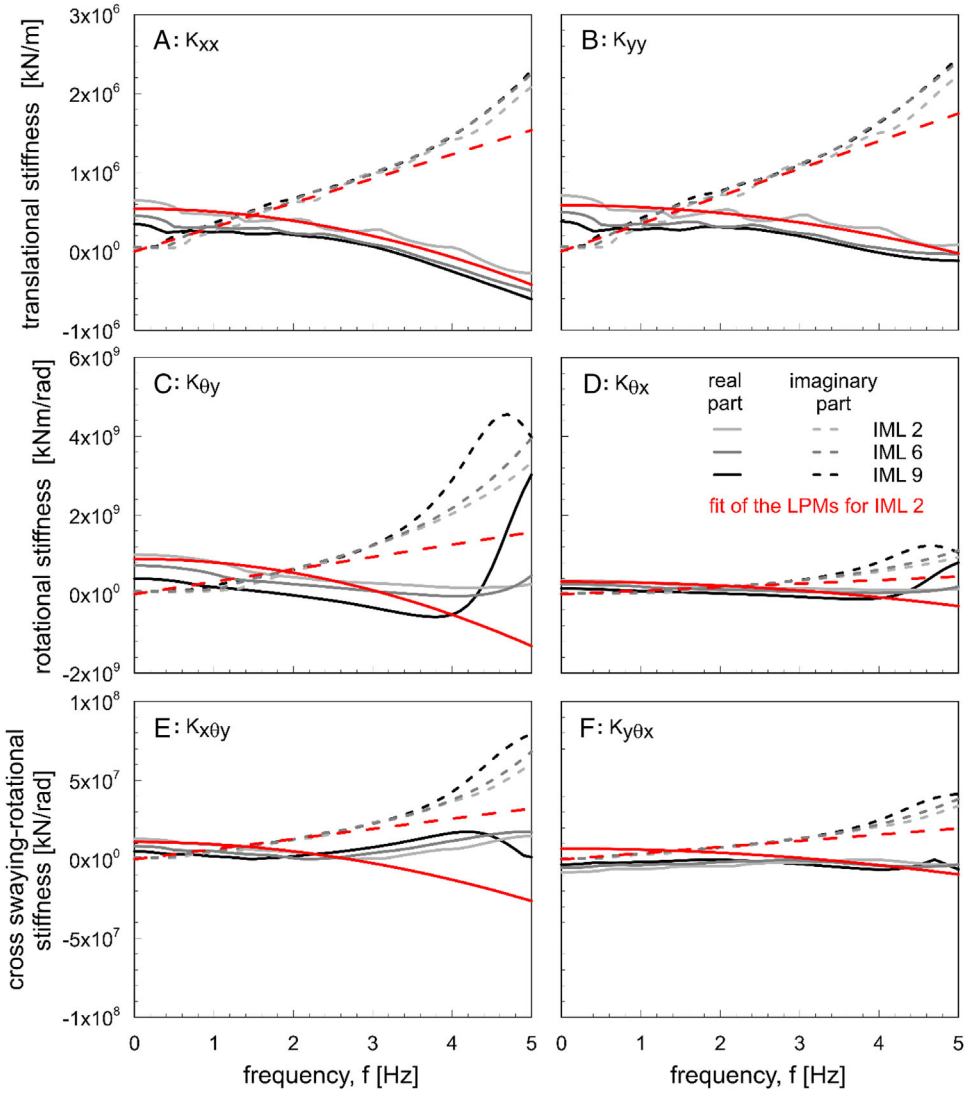

FIGURE 10 Impedance functions of the pile group for intensity measure levels (IMLs) 2, 6, and 9

of the subsoil in shearing oscillations), the effect of radiation damping is prevailing, and the imaginary part varies almost linearly with the frequency excitation.

The functions plotted in Figures 9 and 10 formed the basis for the calibration of the LPMs. The first step consists of choosing a functional form for the approximation of the actual impedance functions. As shown by the superimposed fit for the IML 2 in Figures 9 and 10, this was chosen to be parabolic for the real part and linear for the imaginary component. The generic impedance function, K_{ij}, (where degrees of freedom ij can coincide, as in the translation or rotation terms, or differ, as in the coupled term) is then represented as:

$$K_{ij}(\omega) = \mathrm{Re}\left[K_{ij}(\omega)\right] + \mathrm{Im}\left[K_{ij}(\omega)\right] = \left(k_{ij} - \omega^2 m_{ij}\right) + jc_{ij}\omega \tag{1}$$

where the constant terms k_{ij}, m_{ij} and c_{ij} are determined through least square fit over the frequency range of interest. This procedure is carried out at each chosen IML to reflect the reducing stiffness and increasing damping as the IML increases. Depending on the capabilities of the FE program used for structural analysis, it may be necessary to carry out a further step in order to introduce the translation-rotation coupling, as in this work (in particular, it was not possible to assign cross-mass terms to a node). A modified version of the Carbonari et al.[12] model, where the translational mass, spring and damper are split at the ends of a rigid bar to introduce translational-rotational coupling, was adopted.[42] The same model was also suggested by Carbonari et al.[43] together with predictive formulae for the relevant parameters, thus avoiding the need for preliminary analysis of the soil-foundation system to establish the impedances functions but, similarly to those by,[11] these

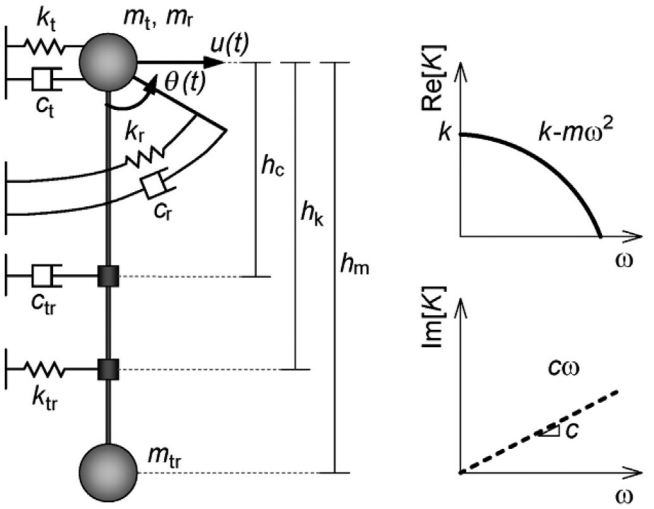

FIGURE 11 Assembly of springs and viscous dampers build up to idealize the foundation behaviour

expressions can be used only for homogeneous soils. In this modified version of the LPM three independent heights (h_{m}, h_{k} and h_{c} in Figure 11) are defined to simultaneously match the frequency dependency of translational, rotational and coupled terms of the real (stiffness) and imaginary (damping) parts of the fitted impedance functions. This second step of the calibration process is described in the following.

The LPM has three degrees of freedom, $\{u, \theta, u^*\}$. Only the first two are independent (due to the kinematic constraint imposed by the rigid bar) and coincide with those for which the 2×2 mass, stiffness and damping matrices $[m_{ij}]$, $[k_{ij}]$ and $[c_{ij}]$ have been derived above. The relationship between these matrices, which are known from the least square fit of the impedances evaluated with Dynapile, and the unknown parameters of the LPM can be found from the rigid constraint:

$$\begin{Bmatrix} u \\ \theta \\ u^* \end{Bmatrix} = \begin{bmatrix} 1 & 0 \\ 0 & 1 \\ 1 & h \end{bmatrix} \begin{Bmatrix} u \\ \theta \end{Bmatrix} \tag{2}$$

It is therefore possible to write that:

$$\begin{bmatrix} 1 & 0 & 1 \\ 0 & 1 & h \end{bmatrix} \begin{bmatrix} m_t & 0 & 0 \\ 0 & m_r & 0 \\ 0 & 0 & m_{tr} \end{bmatrix} \begin{bmatrix} 1 & 0 \\ 0 & 1 \\ 1 & h \end{bmatrix} = \begin{bmatrix} m_t + m_{tr} & hm_{tr} \\ hm_{tr} & m_r + h^2 m_{tr} \end{bmatrix} = \begin{bmatrix} m_{11} & m_{12} \\ m_{12} & m_{22} \end{bmatrix} \tag{3}$$

which gives three equations for the mass terms:

$$m_{tr} = m_{12}/h \tag{4}$$

$$m_t = m_{11} - m_{12}/h \tag{5}$$

$$m_r = m_{22} - m_{12}h \tag{6}$$

Some additional considerations impose some constraints, an example of which is reported again for the mass terms:

$$m_{11} > 0, m_{22} > 0, m_{12}^2 < m_{11}m_{22} \tag{7}$$

$$m_{tr} > 0 \rightarrow m_{12} > 0, m_t > 0 \rightarrow h > \frac{m_{12}}{m_{11}}, m_r > 0 \rightarrow h < \frac{m_{12}}{m_{22}} \tag{8}$$

TABLE 3 Lumped parameters for the case study of Napoli

IML	direction	m_t [kN/g]	m_r [kN/g]	m_{tr} [kN/g]	k_t [kN/m]	$k_r 10^{-3}$ [kNm]	k_{tr} [kN]	c_t [kNs/m]	$c_r 10^{-3}$ [kNms]	c_{tr} [kNs]	h_m [m]	h_k [m]	h_c [m]
2	X	1896	815138	1491	1639900	426569	565633	64726	13621	49949	31.25	31.85	21.98
6	X	856	968088	972	1210310	218005	309612	64379	12985	47363	46.11	29.74	21.81
9	X	402	528945	907	949353	150632	219249	56206	12705	36529	43.58	29.08	23.96
2	Y	1960	237412	1517	1686250	155505	613897	64389	3895	59079	16.66	18.59	11.24
6	Y	942	303160	957	1235360	82663	359722	66498	3926	53372	25.27	17.23	11.52
9	Y	509	203857	822	980691	59126	247327	58110	3866	40631	25.46	17.30	12.72

TABLE 4 Lumped parameters for the case study of Piana del Fucino (L'Aquila)

IML	Direction	m_t [kN/g]	m_r [kN/g]	m_{tr} [kN/g]	k_t [kN/m]	$k_r 10^{-3}$ [kNm]	k_{tr} [kN]	c_t [kNs/m]	$c_r 10^{-3}$ [kNms]	c_{tr} [kNs]	h_m [m]	h_k [m]	h_c [m]
2	X	200.1	381090	775.45	323975	333794	217930	19482	14222	29427	48.95	50.62	34.8
6	X	120.1	246015	641.89	245749	243735	120009	21749	15911	30285	49.31	54.98	35.5
9	X	339.6	735308	223.49	264446	147071	20317	23204	16158	30192	73.86	88.29	35.1
2	Y	103.8	90097.5	513.53	345218	118011	237693	18676	3585	36858	32.31	28.95	17.0
6	Y	27.4	30832.8	407.22	261235	87296	136215	21934	4236	36856	34.68	31.23	17.6
9	Y	71.1	137348	142.93	284929	56029	24206.5	24104	4502	35967	53.79	50.11	17.7

As a matter of fact, when using a single height h for the position of m_{tr}, k_{tr} and c_{tr} along the rigid link, there are often cases where the set of constraints does not leave any feasible value for h.It is preferable to use three distinct values h_m, h_k and h_c (Figure 11). The complete set of coefficients of the LPMs are synthesized in Tables 3 and 4 pertaining to the sites of Naples and L'Aquila, respectively. Noteworthy, the earthquake intensity level has a very small influence on the viscous coefficient representing the effect of radiation damping in each vibration mode.

3.2 | Simplified non-linear inertial macro-element

In an attempt to develop a model capable of describing the non-linearity in the soil-foundation system while keeping the capability of accounting for radiation damping and frequency dependence of stiffness, the linear springs are replaced by a single intensity-independent non-linear hysteretic spring. Since coupling between the swaying and rocking motions is disregarded, four independent lumped plasticity models are adopted for translation and rotation (two in each of the two orthogonal planes XZ and YZ of the buildings). The assumed plasticity law is the classical BW formulation:

$$F = a\frac{F_y}{u_y}u + (1-a)F_y z \tag{9}$$

$$\dot{z} = \frac{A - |z|^n [\gamma + \beta \mathrm{sgn}(\dot{u}z)]}{u_y}\dot{u} \tag{10}$$

where F_y is the generalized yield force, u_y is the work-conjugate yield displacement, a is the ratio between the final tangent stiffness and the elastic stiffness, A is a parameter determining the tangent stiffness, while (β, γ, n) are dimensionless parameters controlling the hysteretic behaviour. The restoring force is composed by two contributions, the linear elastic component and the hysteresis component. In order to satisfy the thermodynamic admissibility, the accordance with Drucker's postulate and the uniqueness conditions, the following inequalities must hold[44]:

$$\begin{aligned} &\beta > 0, -1 < \eta < 1, n \geq 1 \\ &\gamma = \eta\beta \end{aligned} \tag{11}$$

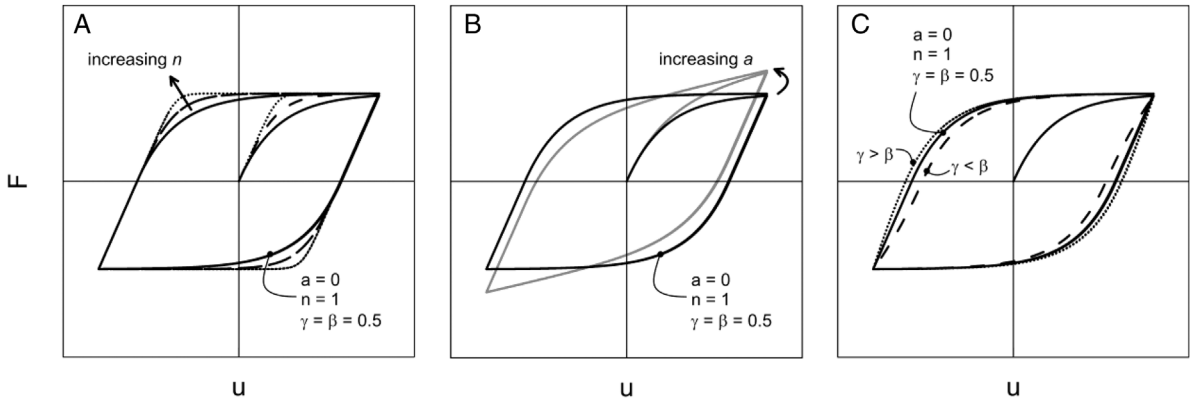

FIGURE 12 The Bouc-Wen constitutive relationship

TABLE 5 Bouc-Wen model parameters for the case of Piana del Fucino

Direction	H_u [MN]	M_u [MNm]	k_t [MN/m]	k_r [MNm/rad]	m_t [kN/g]	m_r [kN/g]	A	a	β	γ
X	17.42	194	542	8.92E + 06	976	2.24E + 06	1	0	0.5	0.5
Y	17.42	126	583	3.17E + 06	617	0.63E + 06	1	0	0.5	0.5

The influence of (n, a, η) on the response of the BW model is depicted in Figure 12. For small values of the exponential parameter n, the transition from elastic to the post-elastic branch is smooth, while for large values this transition becomes abrupt, with the assembly of springs approaching a bi-linear behaviour (Figure 12A). If $a = 0$, the contribution of the elastic spring to the restoring force is also zero (Figure 12B). Finally, Figure 12c elucidates the role of parameter η controlling the size and the shape of the hysteretic loop. Tangent stiffness parameter A is commonly set to unity to eliminate redundancy,[45] therefore, according to Constantinou and Adnane[46]:

$$\frac{A}{\gamma + \beta} = 1 \rightarrow \gamma + \beta = 1 \tag{12}$$

Following all the above constraints, the overall number of unknown parameters reduces to (F_y, u_y, a, n, η). The identification of the BW parameters is usually performed by comparing the model output and a benchmark undertaken by model experiments or advanced numerical analyses. A review of the different algorithms proposed in literature can be found in Chang et al.[47] For the purpose of this study, reference is made to the flow chart proposed by Kunnath et al.[48] in which the yield values (F_y, u_y) and the post-yield stiffness a are first determined and the hysteresis model is then calibrated using a least-square iterative Gauss-Newton fit.

The calibration of the BW models has been carried out only for the case study of Piana del Fucino. A preliminary analysis of the load sharing between the raft-soil contact and the pile group was carried out using the PDR method,[49] so as to evaluate the proportion of the axial load, Q_p, from the structure carried out by piles. The moment capacity, M_u, was then calculated from Q_p through the interaction diagram suggested by Di Laora et al.[59] The horizontal capacity was calculated from the same axial load by means of the failure envelope in the (Q, H) plane proposed by Iovino et al.,[50] in which the dependence of the lateral capacity of the foundation from the yielding moments of the piles' cross-section is explicitly taken into account. With regard to this last quantity, the longitudinal reinforcement area of the piles was taken equal to 50 cm^2, which is about 1% of the cross sectional area of the pile. The horizontal and moment capacities of the pile group along any direction (H_u, M_u) under the axial load acting upon the pile group are listed in Table 5. The initial tangent stiffness, the viscous damper and the fictitious mass pertaining to each oscillation mode are coincident with those already identified for the LPMs at IML 2, to make the BW model comparable with the LPM at very low strain. The modelling choice proposed in this work is somewhat different from that adopted in other dynamic macro-models[51–53] where the BW spring is attached in series to a complex spring simulating the far-field response. Notably, the damper position in parallel with the BW spring is chosen because radiation effects for pile groups, especially those related to the rotational motion, are governed by the group geometry and the piles' axial response, resulting in a different behaviour from shallow foundations (Cavalieri et al.[60]), where the viscous damper is often attached in series with the non-linear spring modelling local soil inelasticity.

TABLE 6 HSS parameters

c_u [kPa]	E_{50ref} [kPa]	E_{oedref} [kPa]	E_{ur} [kPa]	G_{0ref} [kPa]	γ_{07}	m
55	2288	1830.4	6864	22000	7.46E-04	0.4

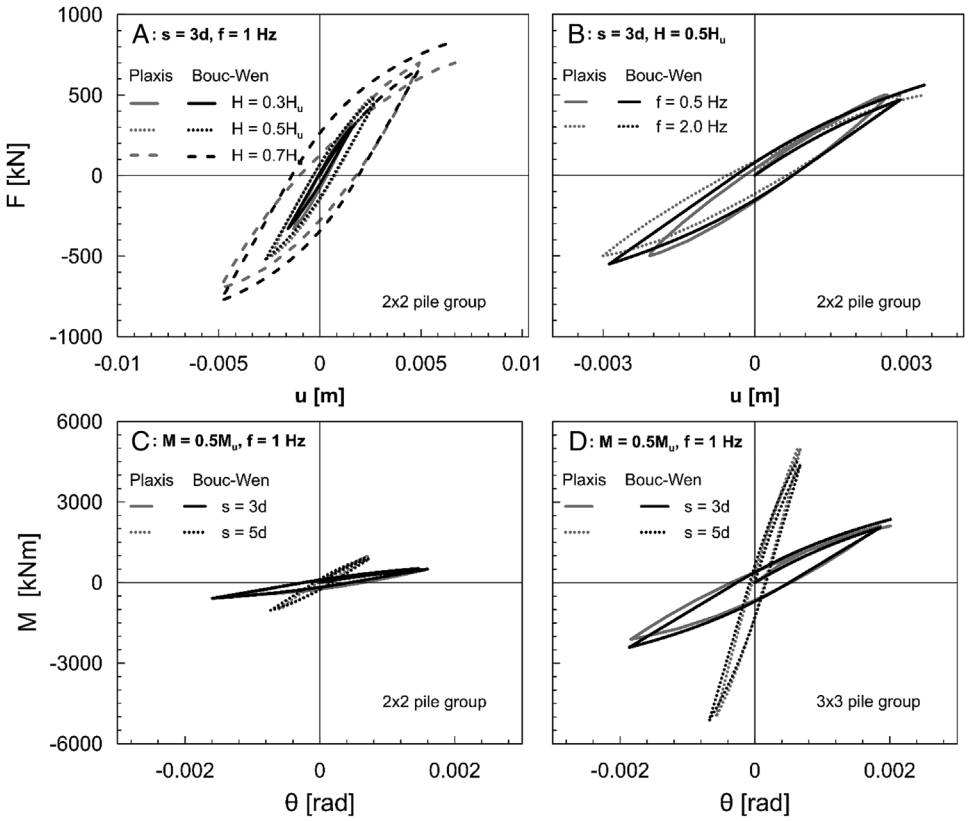

FIGURE 13 Bouc-Wen versus 3D finite element (FE) model

With regard to cyclic parameters, preliminary 3D FE analyses were carried out using code Plaxis 3D[54] by means of the advanced constitutive model Hardening Soil with Small Strain Stiffness which combines the double hardening plasticity model of Vermeer[55] with two additional parameters describing the strain history dependent behaviour of the isotropic elastic stiffness.[56] Soil model parameters were established so as to back-figure the results of resonant column, undrained and drained triaxial tests carried out by Burghignoli et al.[30] at the site of Piana del Fucino and are synthesized in Table 6. Reference is made to the undrained behaviour of four different configurations, to assess the stability of the fitted cyclic parameters: a 2 × 2 or a 3 × 3 pile group, with piles 1 m in diameter and 20 m long, modelled as elastic solid elements and spaced at 3 or 5 diameters. The foundation was excited atop the piles' connecting cap by applying sinusoidal waves with variable amplitude and frequency of either horizontal or moment load. The amplitude of any wave was set equal to a proportion of the yield force, which was evaluated throughout a push-over analysis of the FE model. Figure 13 illustrates the cyclic behaviour of the pile groups predicted by the 3D FE model. Also shown for comparison are the hysteresis loops predicted by the BW model by taking $a = 0$, $n = 1$, $\eta = 1$ and the initial tangent stiffness of the push-over analysis. The agreement between the two models is fully satisfactory for all the examined pile layouts and, hence, the above values were retained for the subsequent non-linear analyses of the reference buildings. A summary of the cyclic parameters of the BW model is reported in Table 5. The basic non-linear macro-element, without the fictitious mass and damper, coincides with the described BW force-displacement law.

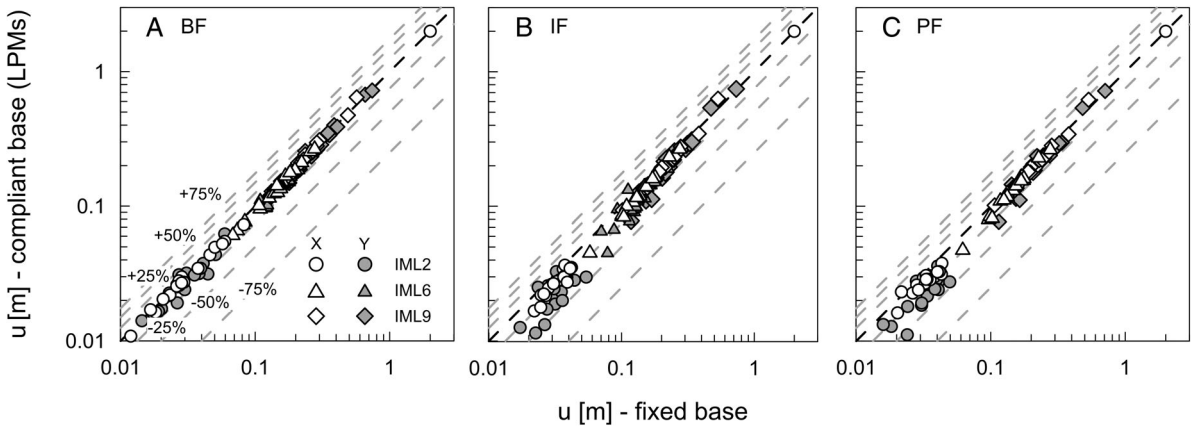

FIGURE 14 Soil-foundation-structure interaction (SFSI) effects predicted by Lumped Parameter Models (LPMs): pyroclastic soil of Naples

4 | ANALYSES RESULTS

4.1 | Visco-elastic LPMs

The ground motion from seismic site response analysis is first expanded in Fourier series and then multiplied by the horizontal impedance of the foundation, as detailed in Pinto and Franchin.[10] The time histories of forces obtained from the inverse Fourier transform of this function is then applied at the interface between the structural model and the assembly of LPMs. This analysis technique is particularly advantageous in that the fictitious masses of the LPMs are not excited by the input motion, ensuring that, in the absence of the structural mass and therefore of the inertial interaction, the motion at the interface node coincides with the foundation input motion. In practice, however, the difference in response with the conventional application of the input excitation as an acceleration time-series at the fixed-side of the LPM is small. This is relevant because a similar approach cannot be easily pursued with a non-linear macro-element.

Figure 14 illustrates the comparison between the seismic demand, expressed in terms of lateral displacement of the roof relative to the base, in the compliant and in the fixed base models for the case study of Naples and IMLs 2, 6 and 9. SFSI effects are almost negligible for the BF building, while they are clearly beneficial for infilled models and IML 2, especially along the Y-direction. For the PF model, as an example, the maximum lateral displacement along Y is reduced by 28%, as an average, while the reduction is 14% for IML 6 and 9% for IML 9 (note that the return period of the IML 6 stripe, shown in Table 2, is 1000 years, thus a reduction of about 20% can be expected for the design level of this residential building). Focusing on structural response, the roof drifts for the medium and high intensity stripes (IMLs 6 and 9) range between 0.1 and 1.0 m. These values, divided by the building height ($H = 27.8$ m), correspond to a maximum roof drift ratio of about 3.6%. This last quantity is a lower bound of the interstorey drift ratio, which is indeed larger, reaching its maximum usually at floors 3 to 5, with an average of about 4% for all models (BF, IF or PF) and peaks for some motions between 6% and 8%. For comparison, the yield interstorey and roof drift ratios at peak moment resistance are on average below 1% and around 5%, respectively, confirming that the structure is elastic for IML 2 and inelastic for IMLs 6 and 9.

If the attention is shifted to the case study of Piana del Fucino (Figure 15), the picture is somewhat similar from a qualitative standpoint, but SFSI effects are more relevant for this softer subsoil. Quantitative results in terms of mean (μ), standard deviation (σ) and coefficient of variation (μ/σ) of the ratio between seismic demand in the compliant base model over that in the fixed base building are summarized in Tables 7 and 8 for sites of Naples and L'Aquila, respectively. In Piana del Fucino case, SFSI effects are more pronounced in terms of both mean reduction and standard deviation. Infill models under low intensity earthquakes (IML 2) in Y-direction represent an exception to this general trend, even if displacement data are particularly scattered, with σ ranging in between 36.9 and 39.9%. The reduction of lateral displacement under low and intermediate intensity levels is due mainly to the radiation damping associated to the swaying motion of the foundation. Such effect, however, has a tendency to vanish with increasing IML for any modelling choice selected for the infills. This result may be attributed to the negligible amount of energy dissipated by the foundation vibration compared to that generated by the hysteresis of the structural members.

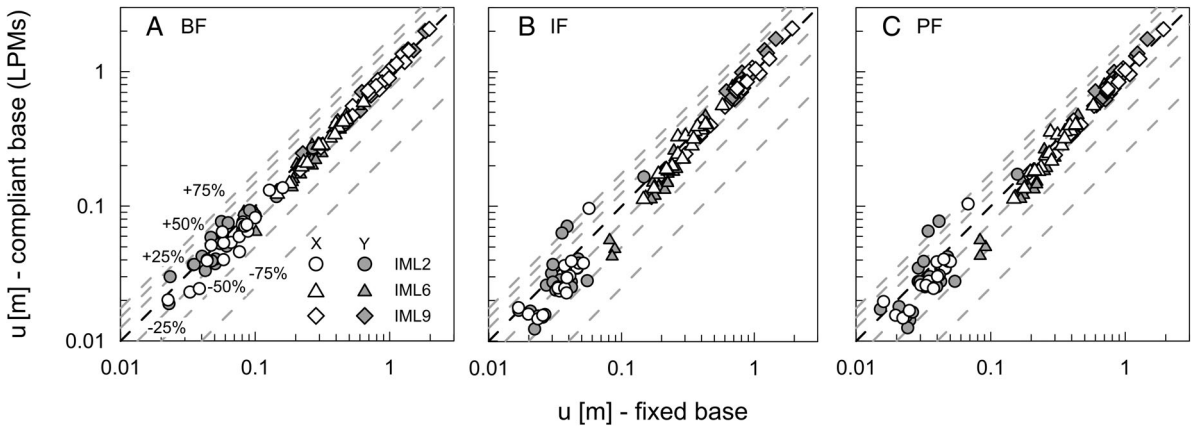

FIGURE 15 Soil-foundation-structure interaction (SFSI) effects predicted by Lumped Parameter Models (LPMs): clay deposit of Piana del Fucino

TABLE 7 Mean, standard deviation and CoV of ratio of displacement of compliant and fixed-base models (Lumped Parameter Models [LPMs], Naples)

		X-direction			Y-direction		
Building model	**IML**	**μ [%]**	**σ [%]**	**CoV**	**μ [%]**	**σ [%]**	**CoV**
BF	2	95.4	4.5	0.05	88.8	11.6	0.13
	6	96.5	4.2	0.04	90.6	6.0	0.07
	9	98.2	4.6	0.05	94.9	6.4	0.07
IF	2	82.6	7.2	0.09	73.4	16.3	0.22
	6	92.8	5.7	0.06	85.5	13.4	0.16
	9	93.8	6.4	0.07	90.0	12.4	0.14
PF	2	84.6	8.1	0.10	71.8	12.7	0.18
	6	93.6	6.1	0.06	86.0	9.8	0.11
	9	94.4	5.9	0.06	90.8	11.5	0.13

TABLE 8 Mean, standard deviation and CoV of ratio of displacement of compliant and fixed-base models (Lumped Parameter Models [LPMs], L'Aquila)

		X-direction			Y-direction		
Building model	**IML**	**μ [%]**	**σ [%]**	**CoV**	**μ [%]**	**σ [%]**	**CoV**
BF	2	85.4	14.0	0.16	98.5	18.7	0.19
	6	94.6	5.2	0.05	91.3	12.9	0.14
	9	97.9	7.3	0.07	99.6	8.7	0.09
IF	2	81.8	23.9	0.29	88.5	36.9	0.42
	6	95.4	12.0	0.13	80.3	17.8	0.22
	9	97.8	9.3	0.09	100.9	14.4	0.14
PF	2	83.9	20.7	0.25	91.5	39.8	0.44
	6	95.1	12.7	0.13	81.0	17.2	0.21
	9	97.9	8.7	0.09	100.2	13.4	0.13

4.2 | Bouc-Wen models

The seismic excitation is applied in this case in the conventional form of a time series of base acceleration, thus involving the excitation of the fictitious mass belonging to the simplified inertial macro-element assembly.

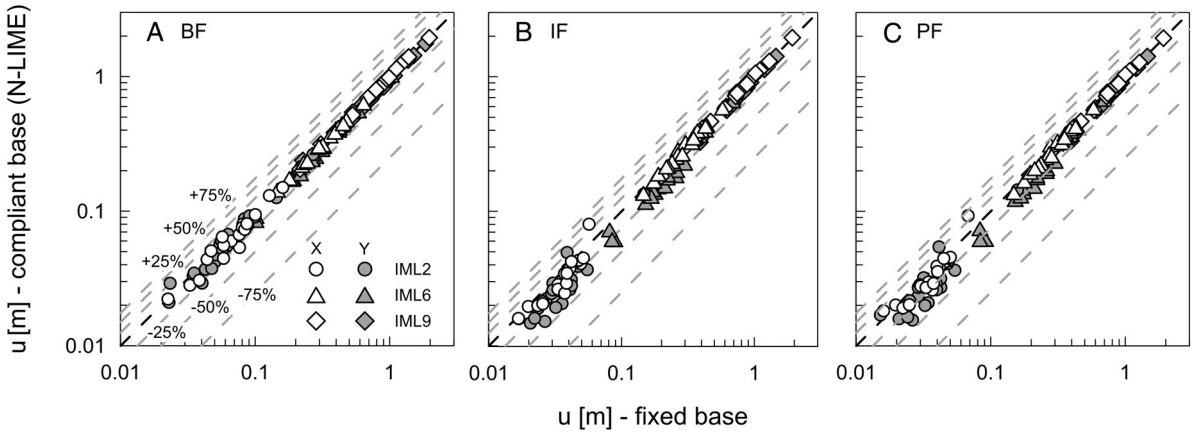

FIGURE 16 Soil-foundation-structure interaction (SFSI) effect predicted by simplified non-linear inertial macro-element (N-LIME) model: clay deposit of Piana del Fucino

TABLE 9 Mean, standard deviation and CoV of ratio of displacement of compliant and fixed-base models (non-linear inertial macro-element [N-LIME], L'Aquila)

		X-direction			Y-direction		
Building model	**IML**	μ [%]	σ [%]	**CoV**	μ [%]	σ [%]	**CoV**
BF	2	92.9	10.2	0.11	95.3	11.8	0.12
	6	99.6	1.8	0.17	93.7	4.7	0.05
	9	100.4	1.8	0.02	95.9	3.2	0.03
IF	2	90.0	14.9	0.17	78.2	16.1	0.21
	6	99.7	4.3	0.04	81.4	7.7	0.09
	9	100.2	3.0	0.03	93.5	4.2	0.05
PF	2	92.7	13.8	0.15	81.2	18.7	0.23
	6	99.5	4.8	0.05	82.3	7.1	0.09
	9	100.1	2.5	0.03	93.8	4.0	0.04

The response of the building on compliant base is compared to that obtained for the fixed base assumption in Figure 16. SFSI effects are, again, more pronounced for infilled buildings at the low intensity level, especially in terms of data scattering, and tend to vanish definitely by increasing the earthquake intensity level. The mean value, the standard deviation and the coefficient of variation of the ratio between the two displacements are summarized in Table 9. In other words, the non-linear behaviour of the foundation has no practical relevance on the seismic performance of the building, indicating that the energy dissipated by hysteresis of structural members is again the prevailing dissipation mechanism. The reduction of seismic demand at the low and intermediate intensity level is smaller than that calculated with the LPMs. A plausible explanation for this attenuated reduction is that cross swaying-rotational effects with BW model are disregarded. Figure 17 illustrates what would be the effect of SFSI without the fictitious mass. The plots in this figure can be hardly distinguished from those obtained with the complete N-LIME model, suggesting that the fictitious mass has only a little influence on the overall seismic demand. If the BW springs are added to the foundation cap without fictitious masses and dampers, the picture is completely different (Figure 18). For all models, especially for the infilled ones in the Y-direction (of lower moment resistance for the foundation), the predicted reduction in structural deformation at the higher intensities is much larger than that associated with the two former modelling strategies. This unconservative overestimation is associated to much larger inelastic rotations, due to the absence of the corresponding damper (translation behaves similarly in the two macro-element models), as shown in Figure 19. This larger inelastic rotation corresponds to a smaller secant stiffness and, hence, to a concentration of plastic deformations at foundation level which reduces the structural damage.

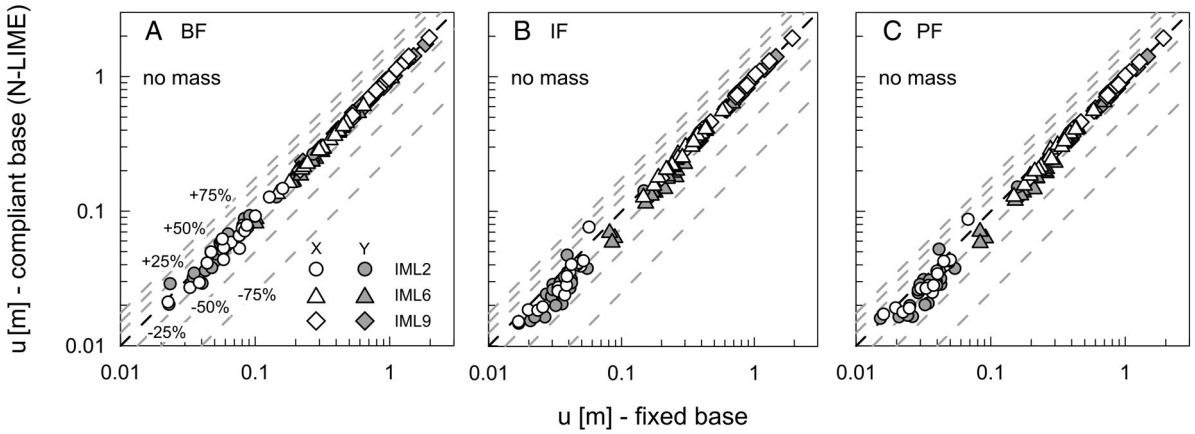

FIGURE 17 Soil-foundation-structure interaction (SFSI) effect predicted by simplified non-linear inertial macro-element (N-LIME) model with no fictitious mass: clay deposit of Piana del Fucino

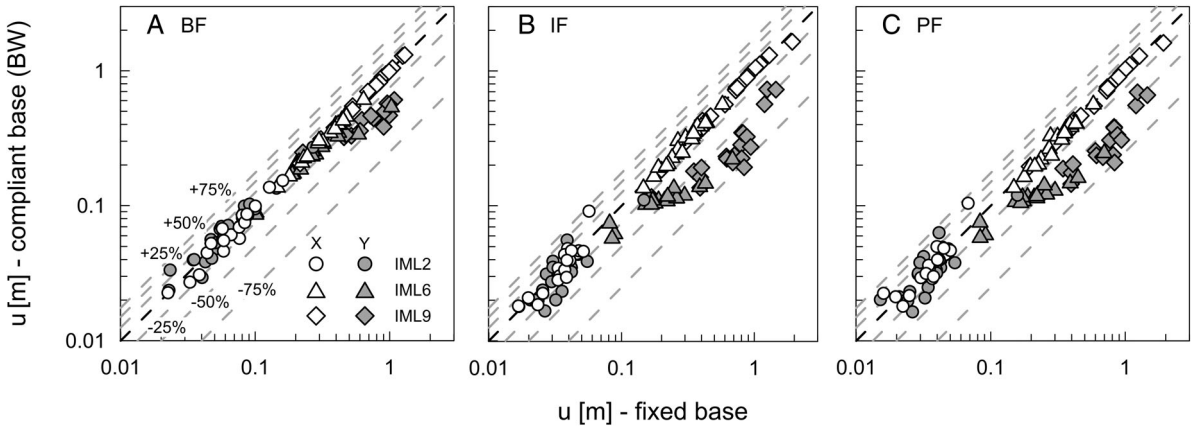

FIGURE 18 Soil-foundation-structure interaction (SFSI) effect predicted by Bouc-Wen model: clay deposit of Piana del Fucino

5 | CONCLUSIONS

This work was aimed at investigating the problem of SFSI for pile supported buildings in non-linear regime. Two interacting models were considered: (a) an assembly of elastic springs, viscous dampers and fictitious masses, capable to approximate the frequency dependent and coupled behaviour of the foundation stiffness, referred to as LPMs; (b) uncoupled BW, assembled with a damper and fictitious mass, referred to as simplified nonlinear inertial macro-element (N-LIME). They were applied to the case study of a nine-storey residential building (with or without infills) in the framework of a Multi Stripe Analysis, with ground motion time series selected at three different earthquake intensity levels according to the Conditional Spectrum method. Two real subsoils were considered, a pyroclastic deposit and a deep layer of lacustrine clay.

For LPMs, a set of foundation impedances along with any oscillation mode of the foundation is first calculated for each considered IML by taking soil stiffness and damping ratio compatible with the level of shear strain mobilized by the passage of seismic waves. For the simplified N-LIME, a single set of static and cyclic parameters along with any oscillation mode of the foundation is determined. The lateral and moment capacity of the foundation are calculated from recent solutions for failure envelopes of pile groups in (Q, M) and (Q, H) planes. Cyclic parameters are calibrated from dynamic 3D FE analyses of square groups of piles carried out with an advanced constitutive model of soil behaviour. Compared to previous works focused on dynamic, non-linear macro-models for SFSI, the frequency dependent behaviour of the foundation stiffness is explicitly accounted for in this case through the fictitious mass attached to the BW spring.

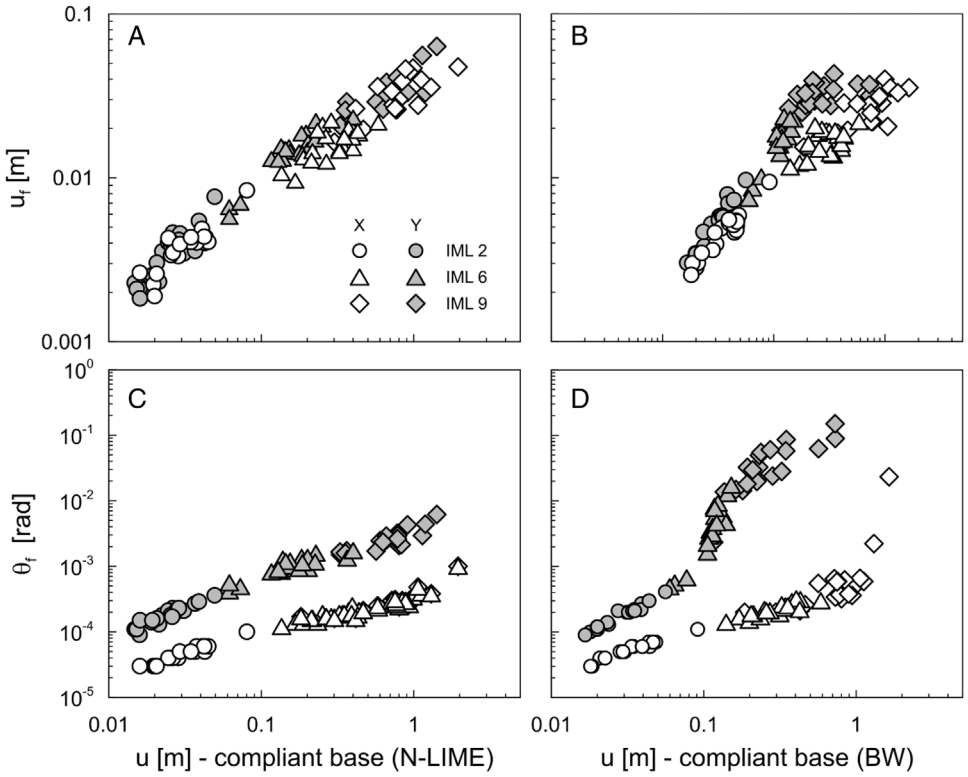

FIGURE 19 Horizontal displacement (A, B) and rotation (C, D) of the foundation versus structural displacement for the selected SFSI models (non-linear inertial macro-element [N-LIME] and Bouc-Wen [BW])

As a general trend, LPMs lead to a remarkable reduction of the lateral displacement at the lowest intensity level (IML 2), especially for building types with the infills, for which the average ratio of the seismic demand in the compliant base model over that in the fixed base one may achieve 28%. Such a behaviour is mainly attributed to the energy dissipated by radiation damping through the swaying motion of the piled foundation. SFSI effects are more scattered for the soft clay layer and have a tendency to vanish by increasing the IML.

Moving to the N-LIME model the picture is very similar, at least qualitatively, with SFSI effects being negligible at the highest IML 9. The non-linearity of the foundation behaviour has only a small effect on the seismic demand in the building, as the foundation response is still in the elastic regime. If the fictitious mass and the additional damper simulating the mechanism of energy dissipation by radiation are removed from the N-LIME assembly, the situation is completely different. In this case, there is a remarkable reduction of the seismic demand at the highest intensity levels in infilled types along with the weak direction (40.5% on average for IF model and IML 9, as an example). Such a reduction is due to the accumulation of plastic rotations at foundation level where, due to the absence of the damper, the moment component is equilibrated only by the rotational spring. The prediction of SFSI effects based on this last modelling choice is obviously not conservative.

The modelling strategies discussed in this work can be easily employed in practice. The moment and lateral capacity of the pile group may be calculated even by hand calculation for example from the failure envelope expressions suggested by Di Laora et al.[59] and Iovino et al.,[50] respectively, while the cyclic parameters of the BW model can be taken coincident with that evaluated in this work, at least in soft soils. The crucial and most difficult issue is the evaluation of the impedance function, from which the fictitious mass and the viscous coefficient of the additional damper are evaluated. To this aim, for the very rare situation of homogenous soil conditions, reference can be made to the regression formulas by Carbonari et al.;[43] for non-homogeneous soils, that is, the majority of practical situations, the evaluation of the impedance function by dynamic analysis with codes like Dynapile is mandatory.

All the above results should be taken in due consideration for a reliable and sustainable assessment of the seismic performance of pile supported buildings. Further research is however needed to investigate subsoil conditions and structural models other than those examined in this work to generalize the above conclusions.

ACKNOWLEDGEMENTS

This research has been developed under the auspices of research projects ReLUIS 2019-2021, granted by Dipartimento della Protezione Civile. Prof. Iunio Iervolino of University of Napoli Federico II is also gratefully acknowledged for his valuable support to this study.

ORCID

Raffaele Di Laora https://orcid.org/0000-0002-9993-5353
Paolo Franchin https://orcid.org/0000-0002-1995-0415

REFERENCES

1. Veletsos AS, Meek JW. Dynamic behaviour of building-foundation systems. *Earthq Eng Struct Dyn*. 1974;3(2):121-138.
2. Veletsos AS, Nair VV. Seismic interaction of structures on hysteretic foundations. *J Struct Div ASCE*. 1975;101(1):109-129.
3. Bilotta E, de Sanctis L, Di Laora R, d'Onofrio A, Silvestri F. Importance of seismic site response and soil-structure interaction in the dynamic behavior of a tall building founded on piles. *Géotechnique*. 2015;65(5):391-400.
4. Parmelee RA. Building-foundation interaction effects. *J Eng Mech Div ASCE*. 1967;93(EM2):131-162.
5. Makris N, Gazetas G, Delis E. Dynamic soil-pile-foundation-structure interaction: records and predictions. *Géotechnique*. 1996;46(1):33-50.
6. de Sanctis L, Iovino M, Di Laora R, Aversa S. Relevance of soil-foundation-structure interaction for pile-supported building. *J Geotech Geoenviron Eng ASCE*. 2020;146(6):04020034.
7. Russo G, Viggiani C, de Sanctis L, Piles as settlement reducers: a case history. *Proc. The Skempton Conference 'Advances in Geotechnical Engineering'*. ICE. London; 2004. pp. 1143-1154
8. Wolf JP. Consistent lumped-parameter models for unbounded soil: physical representation. *Earthq Eng Struct Dyn*. 1991;20(1):11-32.
9. Lesgidis N, Oh-Sung K, Sextos A. A time-domain seismic SSI analysis method for inelastic bridge structures through the use of a frequency-dependent lumped parameter model: a time-domain seismic SSI analysis method for bridge structures. *Earthq Eng Struct Dyn*. 2015;44(13):2137-2156.
10. Pinto EP, Franchin P. Issues in the upgrade of Italian highway structures. *J Earthq Eng*. 2010;14:1221-1252.
11. Taherzadeh R, Clouteau D, Cottereau R. Simple formulas for the dynamic stiffness of pile groups. *Earthq Eng Struct Dyn*. 2009;38(15):1665-1685.
12. Carbonari S, Dezi F, Leoni G. Nonlinear seismic behaviour of wall-frame dual systems accounting for soil-structure interaction. *Earthq Eng Struct Dyn*. 2012;41:1651-1672.
13. Carbonari S, Dezi F, Gara F, Leoni G. Seismic response of reinforced concrete frames on monopile foundations. *Soil Dyn Earthq Eng*. 2014;67:326-344.
14. Sextos AG, Mylonakis GE, Mylona EKV. Rotational excitation of bridges supported on pile groups in soft or liquefiable soil deposits. *Comput Struct*. 2015;155:54-66.
15. Di Laora R, Grossi Y, de Sanctis L, Viggiani GMB. An analytical solution for the rotational component of the foundation input motion induced by a pile group. *Soil Dyn Earthq Eng*. 2017;97:424-438.
16. CEN (European Committee for Standardization). *Eurocode 8: Design of Structures for Earthquake Resistance. Part 5: Foundations, Retaining Structures and Geotechnical Aspects*. CEN (European Committee for Standardization); 2003. EN1998-5.
17. Goit CS, Saitoh M, Mylonakis G, Kawakami H, Oikawa H. Model tests on horizontal pile-to-pile interaction incorporating local non-linearity and resonance effects. *Soil Dyn Earthq Eng*. 2013;48:175-192.
18. Seed HB, Lysmer J, Hwang R. Soil-structure interaction analysis for evaluating seismic response. *J Geotech Eng Div ASCE*. 1975;101(5):439-457.
19. Desai CS, Phan HV, Perumpral JV. Mechanics of three-dimensional soil-structure-interaction. *J Eng Mech Div ASCE*. 1982;108(5):731-747.
20. Curras CJ, Boulanger RW, Kutter BL, Wilson DW. Dynamic experiments and analyses of a pile-group-supported structure. *J Geotech Geoenviron Eng*. 2001;127(7):585-596.
21. Callisto L, Rampello S, Viggiani GMB. Soil-structure interaction for the seismic design of the Messina Strait Bridge. *Soil Dyn Earthq Eng*. 2013;52:103-115.
22. Bouc R. A mathematical model for hysteresis. *Acta Acust United Acust*. 1971;24(1):16-25.
23. Wen YK. Method for random vibration of hysteretic systems. *J Eng Mech Div ASCE*. 1976;102(2):249-263.
24. Italian Ministry for Infrastructures. *D.M. 14 Gennaio 2008, Norme tecniche per le costruzioni. Gazzetta Ufficiale della Repubblica Italiana N. 29, 4 Fe*bbraio 2008. Italian Ministry for Infrastructures; 2008.
25. McKenna F. OpenSees: a framework for earthquake engineering simulation. *Comput Sci Eng*. 2011;13(4):58-66. http://opensees.berkeley.edu.
26. Ricci P, Manfredi V, Noto F, et al. Modeling and seismic response analysis of Italian code-conforming reinforced concrete buildings. *J Earthq Eng*. 2018;22(sup2):105-139.
27. Rippa F & Vinale F. Experiences with CPT in eastern Napoli area. Proc. 2nd European Symposium on penetration testing (ESOPT). Amsterdam, CRC Press. London; 1983.
28. Vinale F. Caratterizzazione del sottosuolo di un'area campione di Napoli ai fini di una microzonazione sismica. *Riv Ital di Geotecnica*. 1988;22(2):77-100.

29. Wehling TM, Boulanger RW, Arulnathan R, Harder LF Jr, Driller MW. Non-linear dynamic properties of a fibrous organic soil. *J Geotech Geoenviron Eng*. 2003;129(10):929-939.
30. Burghignoli A, Cavalera L, Chieppa V, Jamiolkowski M, Mancuso C, Marchetti S, Pane V, Paoliani P, Silvestri F, Vinale F & Vittori E. Geotechnical characterization of Fucino clay. Proc. X ECSMFE. Florence; 1991;1:27-40.
31. Mayne P, Rix G. G_{max}-q_c relationships for clays. *Geotech Testing J*. 1993;16(1):54-60.
32. Konder RL, Zelasko JS, Hyperbolic stress-strain formulation of sands. *Proc. 2nd Pan American Conference on Soil Mechanics and Foundation Engineering*. Sao Paulo, Brazil; 1963;1:289-324.
33. Vucetic M, Dobry R. Effect of soil plasticity on cyclic response. *J Geotech Eng*. 1991;117(1):89-107.
34. ITACA 3.1. *Italian Accelerometer Achive, INGV*. ITACA 3.1; 2020. http://itaca.mi.ingv.it
35. NGA West 2. *NGA West 2 Database, Peer Earthquake Engineering Research Center*. NGA West 2; 2014. http://ngawest2.berkeley.edu.
36. Lin T, Harmsen SC, Jack Wesley Baker JW, Luco N. Conditional spectrum computation incorporating multiple causal earthquakes and ground-motion prediction models. *Bull Seismol Soc Am*. 2013;103(2):1103-1116.
37. Iervolino I, Spillatura A, Bazzurro P. Seismic reliability of code-conforming Italian buildings. *J Earthq Eng*. 2018;22(sup2):5-27.
38. Kottke AR, Rathje EM. Strata; 2008. https://www.geoengineer.org/software/101-Strata
39. Ensoft. *Dynapile 3.0. A Program for the Analysis of Piles and Drilled Shafts under Dynamic Loads*. Ensoft Inc.; 2017.
40. Blaney GW, Kausel E & Roesset JM. Dynamic stiffness of piles. Proc. 2nd Int. Conf. Numerical Methods in Geomechanics. Blacksburg; 1976:1001-1012.
41. Kausel E, Whitman RV, Morray JP, Elsabee F. The spring method for embedded foundations. *Nucl Eng Des*. 1978;48(2-3):377-392.
42. RINTC Workgroup. *Results of the 2015–2017 Implicit Seismic Risk of Code-Conforming Structures in Italy (RINTC) project. ReLUIS Report, Rete dei Laboratori Universitari di Ingegneria Sismica (ReLUIS)*. RINTC Workgroup; 2018. http://www.reluis.it/index.php?option=com_contentandview=articleandid=549andItemid=19
43. Carbonari S, Morici M, Dezi F, Leoni G. A lumped parameter model for time-domain inertial soil-structure interaction analysis of structures on pile foundations. *Earthq Eng Struct Dyn*. 2018. 47(11):2147–2171. https://doi.org/10.1002/eqe.3060.
44. Ismail M, Ikhouane F, Rodellar J. The hysteresis Bouc-Wen model, a survey. *Arch Comput Methods Eng*. 2009;16(2):161-188.
45. Charalampakis AE, Koumousis VK. On the response and dissipated energy of Bouc-Wen hysteretic model. *J Sound Vib*. 2008;309(3–5):887-895.
46. MC Constantinou, Adnane MA. *Dynamics of Soil-Base-Isolated Structure Systems: Evaluation of Two Models for Yielding Systems*. Report to NSAF, Department of Civil Engineering, Drexel University; 1987.
47. Chang C-M, Strano S, Terzo M. Modelling of Hysteresis in Vibration Control Systems by means of the Bouc-Wen Model. *Shock and Vibration*. 2016;2016:1–14. https://doi.org/10.1155/2016/3424191
48. Kunnath SK, Mander JB, Fang L. Parameter identification for degrading and pinched hysteretic structural concrete systems. *Eng Struct*. 1997;19(3):224-232.
49. Poulos HG. Piled raft foundations: design and applications. *Géotechnique*. 2001;51(2):95-113.
50. Iovino M, Maiorano RMS, de Sanctis L, Aversa S. Failure envelopes of pile groups under inclined and eccentric load. *Géotechnique Letters*. 2021;11:(4):1–7. https://doi.org/10.1680/jgele.21.00059
51. Pecker A, Paolucci R, Chatzigogos C, Correia AA, Figini R. The role of non-linear dynamic soil-foundation interaction on the seismic response of structure. *Bull Earthq Eng*. 2014;12:1157-1176.
52. Figini R, Paolucci R, Chatzigogos CT. A macro-element model for non-linear soil-shallow foundation-structure interaction under seismic loads: theoretical development and experimental validation on large scale tests. *Earthq Eng StructDyn*. 2012;41(3):475-493.
53. Chatzigogos CT, Figini R, Pecker A, Salençon J. A macroelement formulation for shallow foundation on cohesive and frictional soils. *Int J Numer Anal Methods Geomech*. 2011;35:902-935.
54. Brinkgreve RBJ, Kumarswamy S, Swolfs WM, Waterman D, Chesaru A & Bonnier PG. PLAXIS 2016. PLAXIS bv. 2016.
55. Vermeer PA. A double hardening model for sand. *Géotechnique*. 1978;28(4):413-433.
56. Benz T, Vermeer PA, Schwab R. A small-strain overlay model. *Int J Numer Anal Methods Geomech*. 2009;33(1):25-44.
57. FEMA 1050. *NEHRP Recommended Seismic Provisions for New Buildings and other Structures, Building Seismic Safety Council of the National Institute of Building Sciences*. FEMA 1050; 2015.
58. Goit CS, Saitoh M, Mylonakis G. Principle of superposition for assessing horizontal dynamic response of pile groups encompassing soil non linearity. *Soil Dyn Earthq Eng*. 2016;86:73-83.
59. Di Laora R, de Sanctis L, Aversa S. Bearing capacity of pile groups under vertical eccentric load. *Acta Geotechnica*. 2019;14:(1):193–205. https://doi.org/10.1007/s11440-018-0646-5
60. Cavalieri F, Correia AA, Crowley H, Pinho R. Dynamic soil-structure interaction models for fragility characterisation of buildings with shallow foundations. *Soil Dynamics and Earthquake Engineering*. 2020;132:106004. https://doi.org/10.1016/j.soildyn.2019.106004

How to cite this article: Noto F, Iovino M, Di Laora R, de Sanctis L, Franchin P. Non-linear dynamic analysis of buildings founded on piles: Simplified modelling strategies for soil-foundation-structure interaction. *Earthquake Engng Struct Dyn*. 2021;1–20. https://doi.org/10.1002/eqe.3589